Semester Project

Ball positioning via laser

Luca Brusatin

Fall 2013

Professors : Christophe Salzmann, Colin Jones
Assistants : Milan Korda, Tomasz Gorecki

Ecole Polytechnique Fédérale de Lausanne
Laboratoire d'Automatique

Laboratoire d'Automatique

EPFL STI IGM LA
ME C2 399 (Bâtiment ME)
Station 9
CH-1015 Lausanne

Téléphone : + 41 21 693 11 71
Fax : + 41 21 693 25 74
E-mail : colin.jones@epfl.ch
Site web : http://la.epfl.ch

ÉCOLE POLYTECHNIQUE
FÉDÉRALE DE LAUSANNE

Lausanne, octobre 2013

Projet de semestre M1
Automne 2013

Candidat : **BRUSATIN Luca Aurelio**
Section de Microtechnique

Sujet : **Ball Positioning via Laser**

The aim of this project is to design a new position measurement system (hardware and software) for the babyfoot. This system relies on laser measurements to derive the ball position. The proposed hardware should be interfaced by the existing DAQ board (voltage input). The measurements precision should be in accordance with the requirements for the control part.

Le nombre de crédits réservés au plan d'études pour ce projet est de **douze**.

Dr. Christophe Salzmann
Prof. Colin Jones

Assistants responsables :
KORDA Milan (tél. int. 3 10 59)
GORECKI Tomasz (tél. int. 3 42 20)

Abstract

The laboratory's babyfoot has been equipped with a robotic "arm" that controls one bar. To block shots from the opponents, the robot needs to react quickly. A first version of a ball tracking system has already been implemented using a high-speed camera. This project has the aim to design a ball positioning system using laser scanners. Existing laser positioning systems do not fulfill the requirements, thus a complete ball positioning system via laser is conceived. The resulting system allows for fast ball tracking with a good precision, it is however sensitive to external noise sources, such as fluorescent lighting.

Contents

1 Introduction

The laboratory's babyfoot has been equipped with a robotic "arm" that controls one bar, replacing a human opponent. To react properly, the robot needs to have an accurate and high speed ball-tracking system. Tests showed that a skilled human player can shoot the ball at speeds up to 10 m/s. Currently, the ball positioning is done with a high-speed camera, achieving ball-tracking at 90 Hz. This rate is not sufficient to estimate the trajectory of the ball when it is moving fast.

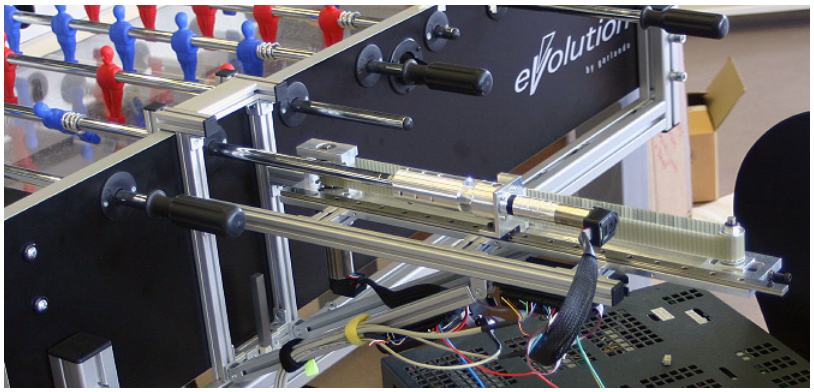

Figure 1.1: Robotic arm mounted on the babyfoot

This project explores the possibility of using laser scanners to do the ball-tracking. The main advantage would be a higher ball-tracking speed than the current camera-based system while keeping the measurements precision in accordance with the requirements for the control of the robot.

The work is separted in two parts. First, the requirements are defined, existing solutions are discussed and the operating principle of a new solution is presented. The second part is focussed on the design and results of this position measurement system.

2 Ball-tracking system

2.1 System requirements

Supposing the ball is perfectly round, the surface flat, neglecting ball-spin and ignoring rebounds on the sides, the ball will follow straight lines between two rows of players. The computer needs to have at least two measurements of the ball position between two rows of players to estimate the trajectory. The required ball-tracking speed can be estimated by measuring typical shot speeds.

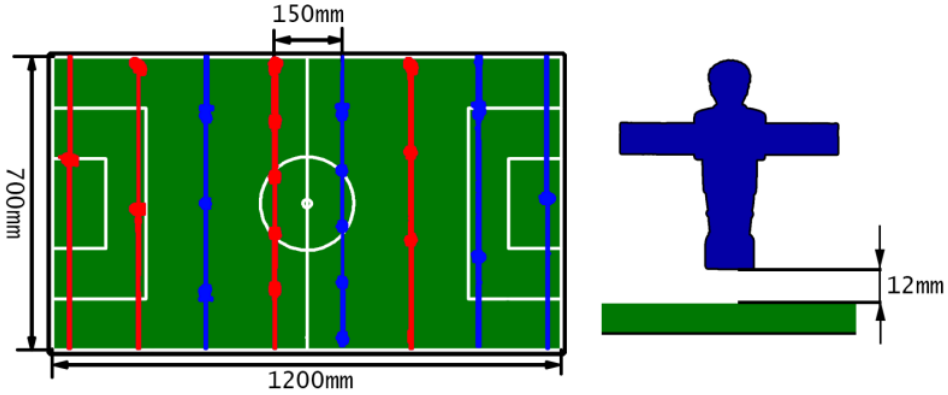

Figure 2.1: Dimensions of the babyfoot

The maximal displacement between two successive position measurements is defined as 75mm, in order to have at least two position measurements between each row (150mm). Different ball speeds have been determined by measuring the delay between the sound produced by the player hitting the ball and the ball hitting the goal. The results are shown in table 2.1.

Shot / Ball speed	Time to move 75mm	Measurement frequency
Weak shot : 1 m/s	75ms	13.3 Hz
Standard shot : 5 m/s	15ms	66.7 Hz
Strong shot : 10 m/s	7.5ms	133 Hz

Table 2.1: Typical shot speeds and corresponding minimal ball-tracking frequency.

A higher position measurement frequency would improve the ball-tracking ability of the robot as it would permit faster reaction to changes. Laser-based tracking solutions measure distances in a plane, thus, in addition to the speed requirements, the system needs to scan in the space available between the surface of the table and the players feet (12 mm), have a field of view of at least 90 ° if placed in the corner of the table, and the operating range should cover the whole table, that is for distances from (close to) 0 mm to 1400 mm (diagonal of the table).

2.2 Existing solutions

There are different methods for distance measurement using lasers. The distance can be obtained from the time of flight of a light pulse sent to a object and reflected back. The distance can also be measured using the phase shift of the reflected light. Other sensors use a lens to focus a reflected spot on a linear photosensitive array. By adding a rotating mirror after a distance sensor, the distances in different directions in a plane can be measured. This is done in LiDAR systems, which are often used in robotics for mapping, localization and obstacle avoidance. The specifications of such a system are shown in table 2.2.

Method	Phase shift
Field of view	70 °
Scanning frequency	180 Hz ... 500 Hz
Angular resolution	0.1 ° ... 1.0 °
Operating range	0.7 m ... 3 m
Error	±3 mm ... ±10 mm
Price	~ 8000 CHF

Table 2.2: Specifications of the SICK LMS400

The SICK LMS400 is the most suitable LiDAR system that could be found. Its scanning frequency is sufficient, however the minimum operating range of 0.7m and the field of view of 70° are not compatible with the dimensions of the babyfoot table, thus a solution specific to the babyfoot is explained in the next section.

2.3 Specific solution

A way to get the position of the ball is scanning a laser in a plane parallel to the surface of the table, in between the surface and the players feet. If the sides of the table are covered in some light absorbant material and the ball is reflective, the laser will be reflected when it crosses the ball. The time of that reflection can be measured and combined with the angle the laser was making at the time to get the angle at which the ball is. By using two such systems, the position of the ball can be triangulated.

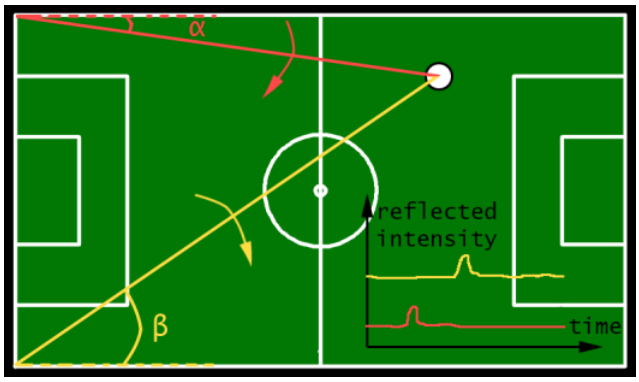

Figure 2.2: Position triangulation using lasers

As in a LiDAR system, the laser beam has to be scanned across the table using a

rotating mirror. However, this system does not need to directly measure the distance with the lasers, which simplifies the detection electronics. The detection circuit needs to measure the light intensity and detect the pulse of light reflected by the ball. By comparing the time elapsed between the crossing by the laser beam of a known reference and the reflected pulse, and knowing the rotating mirror speed, the angle can be determined. To get a precise measurement of the rotating mirror speed, two references, "triggers", can be used, one a the start of the scan sequence, and one at the end. The time elapsed between the crossing of the start trigger and the reflected pulse divided by the time elapsed between the crossing of the start trigger and the stop trigger gives a value that is directly proportional to the angle at which the ball is. That value is also independent of the rotating mirror speed, as long as it is constant. Figure 2.3 shows a scan sequence with placement of the start and stop triggers.

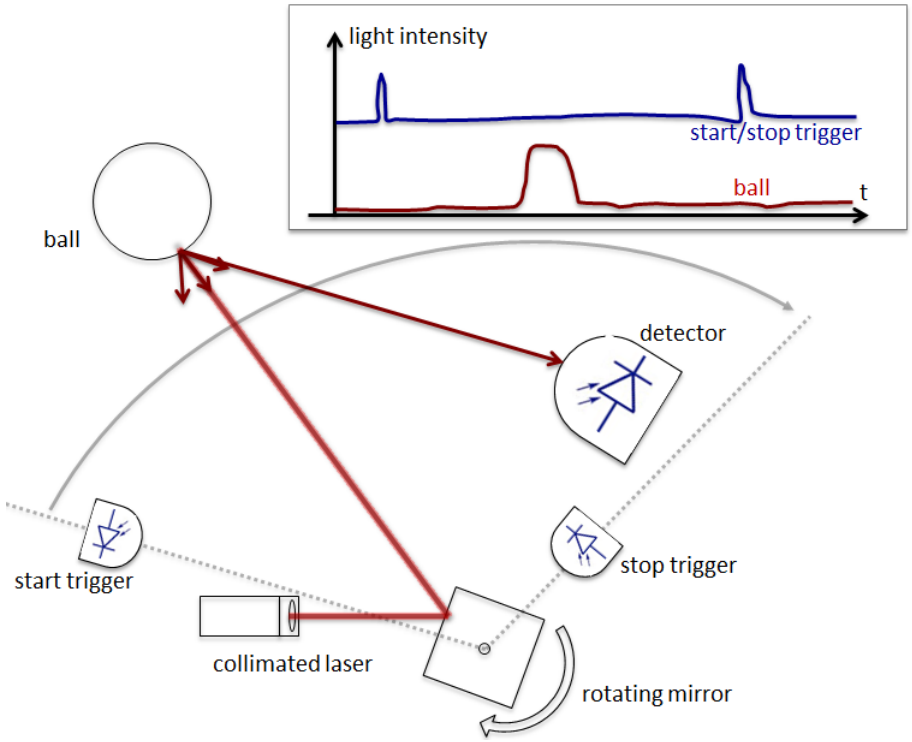

Figure 2.3: Drawing of laser scanner with start and stop triggers

To get the ball position, two scanning systems need to run at the same time, one for measuring each angle (see figure 2.2). To avoid interferences between the two systems, different wavelengths could be used for each system, with matching band-pass filters on the detection circuits. For this semester project, to keep things simple, the two systems will not be running at the same time, switching on and off one after the other. This will avoid the need for more complex optical elements and detection circuits, however the drawback will be a lower ball-tracking speed, as the systems need to scan one after the other. The following chapter will give more details about the achievable scanning speeds.

3 Laser scanner design

3.1 Laser module

3.1.1 Laser safety

Collimated lasers are dangerous to the eyes because of their low divergence : the energy is concentrated in a small ray, that is further concentrated by the lens of the eye and can damage the retina. Laser safety directives at EPFL allow the use of lasers up to class 3R (safety standards IEC 60825-1:2007, ANSI Z136.1:2007), which are considered safe if handled carefully. The ANSI standard explains that "A Class 3R laser system is potentially hazardous under some direct and specular reflection viewing condition if the eye is appropriately focused and stable, but the probability of an actual injury is small. This laser will not pose either a fire hazard or diffuse-reflection hazard."

Figure 3.1: Maximal allowed continous wave power as a function of wavelength. Chart by Danh, CC BY-SA 3.0, en.wikipedia.org/wiki/Laser_safety

For this application, the use of a class 3R laser is considered safe: the laser beam will be scanned at high speed in a horizontal plane slightly above the surface of the table, where it should be impossible to make direct eye contact with the beam. Shiny objects should not be put on the table to avoid specular reflections, but diffuse objects such as a babyfoot ball are not hazardous.

3.1.2 Laser diode

To choose the laser diode, wavelength and optical output power have to be defined. The optical power is limited by the safety regulations, while the wavelength range is defined by the available light detection technology. Photodiodes have the best sensitivity in near-infrared wavelengths (700-1000nm), thus the chosen wavelength will be in that range. A 5 miliwatts, 850 nanometers wavelength laser diode is chosen from Roithner LaserTechnik GmbH in Austria (QL85D6SA). By supplying the diode a forward current of 14 mA, an output power of approximately 3mW will be generated. This is in accordance with the maximal allowed power for a class 3R laser (see figure 3.1).

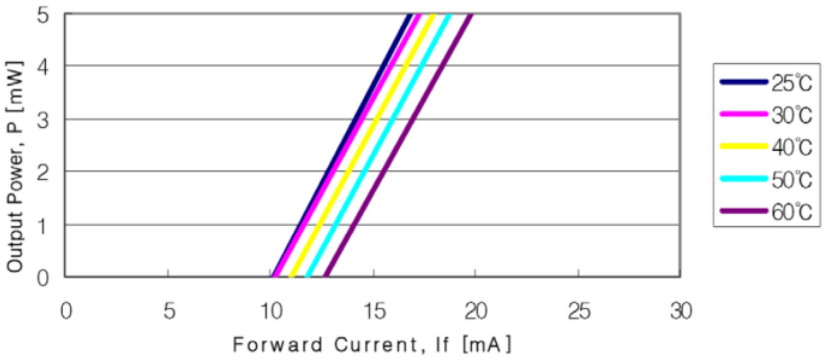

Figure 3.2: Optical output power as a function of forward current. Chart from the QL85D6SA datasheet, Roithner LaserTechnik GmbH.

3.1.3 Laser diode driver

The EU-42 laser diode driver from Roithner LaserTechnik is chosen. It allows modulation of the laser diode for frequencies up to 1 MHz. This is required to be able to quickly switch on and off each laser scanner to avoid interferences from one another, as explained in 2.3. The supply voltage of the driver is between 4 and 6 V. The continuous wave power is set to 3mW by adjusting the supplied current with a potentionmeter situated on the driver. The current is measured with an ammeter in series with the laser diode.

3.1.4 Laser module assembly

In order to have a flexible laser module, teflon sockets and focussable collimating lens modules are bought, also from Roithner LaserTechnik. This allows to mount the laser diode without any soldering inside a module, and permits easy replacement of each part.

Wavelength	850 nm
Optical power	3 mW
Modulable up to	1 MHz
Supply voltage	4 to 6 V DC

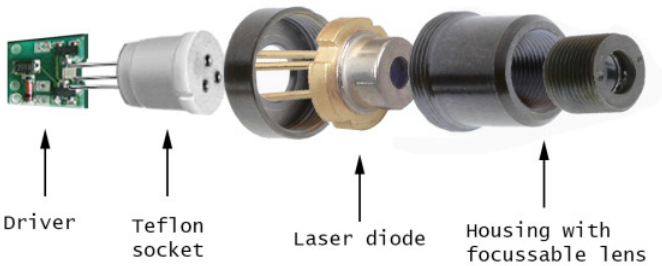

Table 3.1: Laser module specifications.

Note: The case of the laser diode is connected to the laser diode anode (positive supply voltage) and the lens housing is conductive. The module has to be isolated when attached to grounded conductive parts to avoid shorts, see section 3.3.

3.2 Polygon mirror motor

Rotating mirrors are used to scan the laser beams in a plane. The number of facets is important to get the required scan angle. The angle covered by the beam is twice the mirror's rotation (see figure 3.3), thus to get the required scan angle of 90° (see section 2.1), the mirror has to rotate 45°, and a mirror of $360/45 = 8$ sides is suitable. To account for the mirror edges that are not perfect, the beam diameter and the space required by the start and stop triggers, the maximum number of facets is 6 (polygon mirrors commonly have an even number of sides). 6 sides give a total scan angle of $2 \cdot (360/6) = 120°$, leaving some margin for adding start and stop triggers.

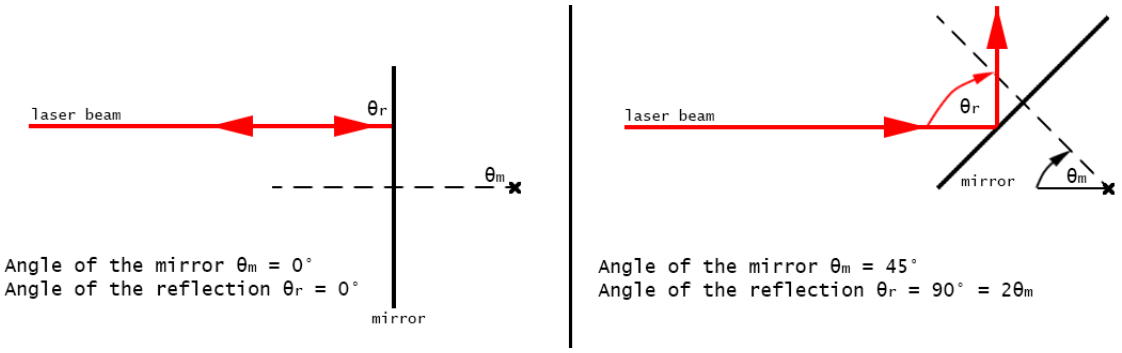

Figure 3.3: The angle of the reflection is twice the angle of the mirror.

Finding polygon scanners is surprinsingly difficult: custom-made units are costly and nothing could be found on different online electronics stores. Polygon mirror motors are however present in all laser printers and a few units were collected from dead or obsolete equipment. Two similar scanners, extracted from HP Laserjet printers, satisfy the requirements and are used in this project. The 4 faceted mirrors give a total scan angle of 180°, leaving a comfortable margin for the placement of the different components although it reduces the duty cycle of the mirror. The duty cycle of a polygon mirror is the used scan angle (90°) divided by the total scan angle available (180°). To have the same scan frequency over the scan angle, a mirror with a lower duty cycle will have to rotate faster. This also means that the laser beam will cross the table (and the ball) faster, requiring a higher bandwidth for the detection circuits.

Supply voltage	8 - 24 V DC
Rotational speed	12 - 45 kRPM
Scan frequency	800 - 3000 Hz
Facets	4
Total scan angle	180°
Used scan angle	90°
Duty cycle	50%

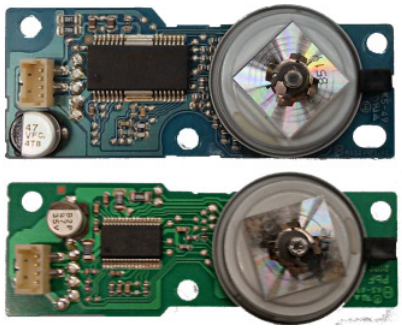

Table 3.2: Specifications of the polygon mirror motors. The scan frequency is 4 times the rotational speed (4 facets).

Note: The two polygon mirror motors boards do not exactly have the same dimensions and are not controlled exactly the same way. The board with the AN44010 chip (green PCB) needs to be periodically reset for an unknown reason (no datasheets could be found, for both units). For more details, refer to the annexes.

3.3 Scanner assembly

Aluminum parts are designed and machined to assemble the different components. The laser module mounted in its bracket can be seen in the center of figure 3.4, wrapped in electrical tape to avoid a short circuit with the grounded aluminum parts. The start and stop triggers consist of photodiodes placed in aluminum tubes. Next to the scanner assembly is the trigger circuit, which transforms the current pulse produced by the trigger photodiodes in a well-defined voltage pulse read by the controller. The laser scanners can be mounted inside the table, on each side of a goal, see figure 3.5

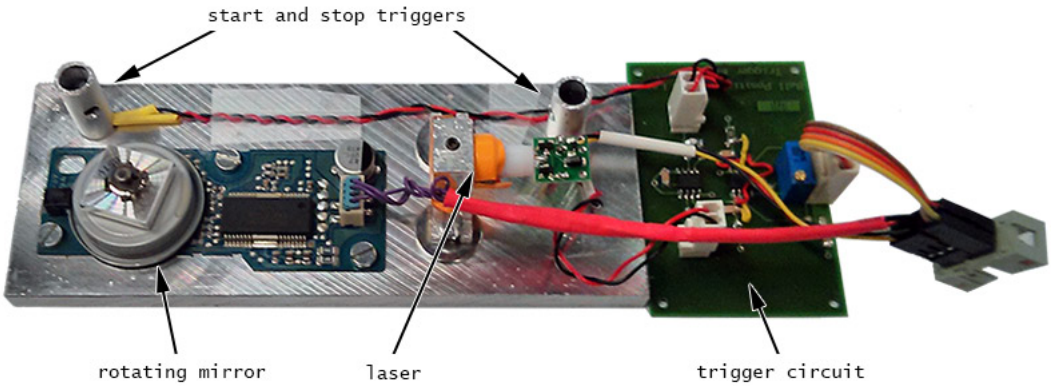

Figure 3.4: Laser scanner assembly, with the trigger circuit on the right.

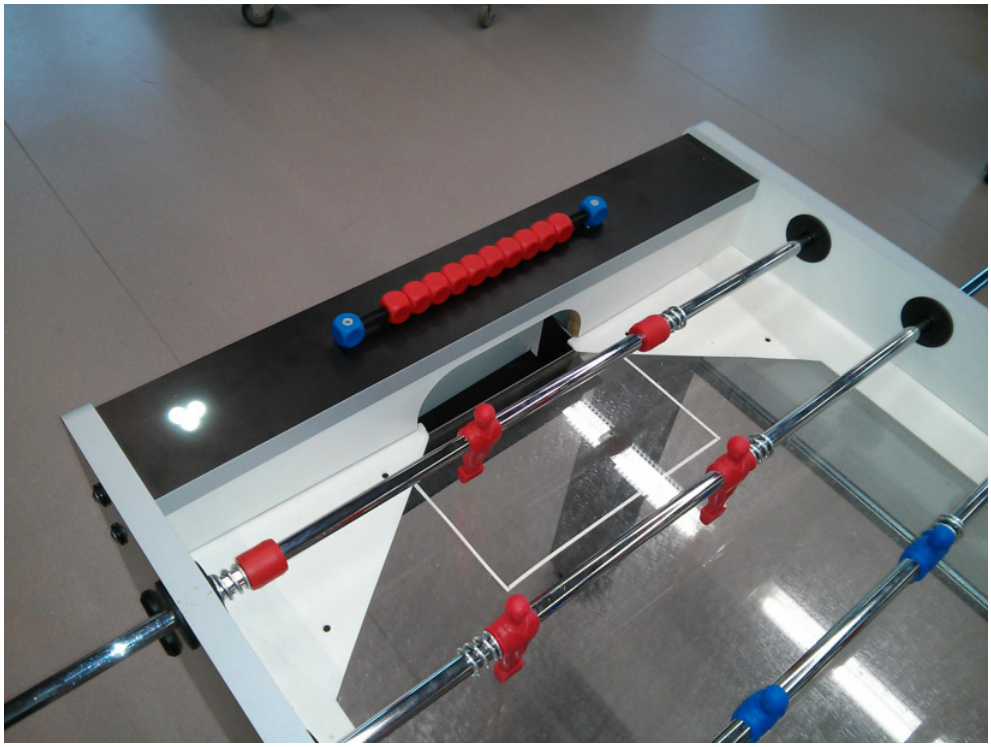

Figure 3.5: End of a babyfoot table.

The laser scanner units are small enough to fit inside the table, on each side of the goal.

4 Laser beam detector circuits

4.1 Ball reflection detector

4.1.1 Principle

A photodiode is used to transform the reflected light into a current, which is converted into voltage by the first amplifier stage, a transimpedance amplifier. The signal is then band-pass filtered and fed to the second stage, a non-inverting operational amplifier. Then, after a low pass filter, the signal is compared to an adjustable reference by a comparator : if the signal is over a certain threshold, the reflected pulse is detected. This signal can be read by the controller. Figure 4.1 shows a simplified circuit. Tests have shown that the sensing range of the detector circuit is limited due to the low laser power available. To cover the entire table, multiple detectors can be placed under the transparent plate already mounted on the babyfoot.

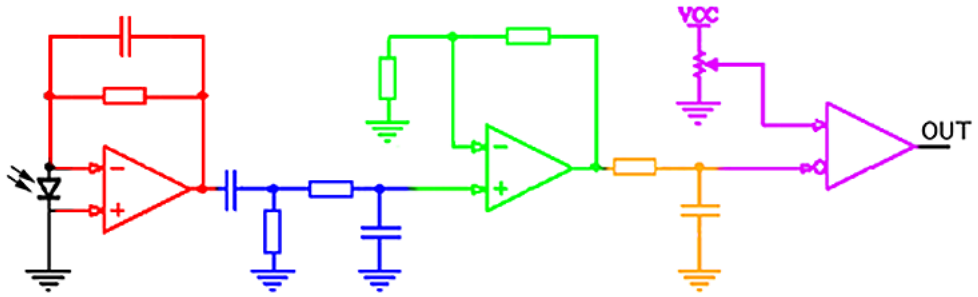

Figure 4.1: Simplified circuit. In red, the first amplifier stage; in blue the band-pass filter; in green the second amplifier stage; in yellow a low pass filter before the comparator (pink).

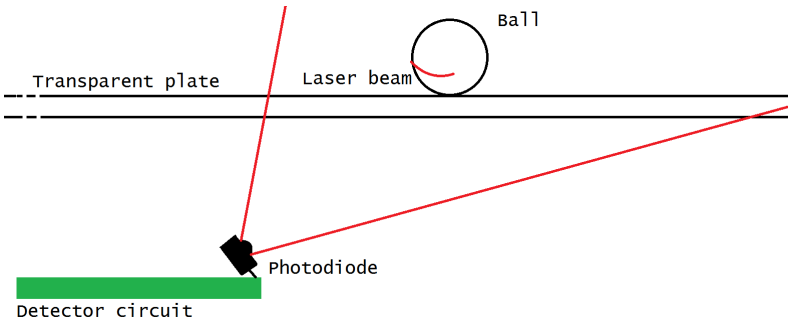

Figure 4.2: Placement of the detector circuit

4.1.2 Components

The Vishay BPV22NF photodiode is chosen for its high sensitivity over the near-IR spectral range, high angle of half sensitivity, big sensitive area, integrated lens and daylight blocking filter.

To choose the transimpedance amplifier (first stage), the required bandwidth needs to be determined. Table 4.1 shows the important parameters and detailed calculations are available in the annexes.

Scan frequency	1 kHZ
Shortest "ball pulse"	6.7 μs
Longest "ball pulse"	247 μs

Highest frequency	148.5 kHz
Lowest frequency	4 kHz

Table 4.1: Summary of the important parameters to design the detection circuit

After different iterations, the scan frequency is set to 1000 Hz, which gives a ball-tracking frequency of 500 Hz. While the polygon mirrors could rotate faster, the detection of the reflection is problematic for higher speeds because of a trade-off between bandwidth and gain in first stage amplifier.

The Microchip MCP632 transimpedance amplifier offers a sufficiently high enough gain-bandwidth product with low noise and can be supplied with a single 5V supply. Two operational amplifiers are included in the same package, allowing to do both amplification stages with the same chip. The LM393 comparator is chosen because it contains two comparator circuits, which will be useful for the trigger circuit. It also has an open collector output, meaning several comparators can be on the same line, pulled up by a single resistor. Thus, the output is a logical OR between all circuits. This allows to have multiple detectors setup in parallel, covering the entire table.

4.1.3 Dimensionning

Starting from the photodiode, the feedback network of the first stage amplifier has to be dimensioned. For this, the photodiode is represented by a current source in parallel with a parasitic capacitance, representing the photodiode capacitance and also the input capacitance of the amplifier.

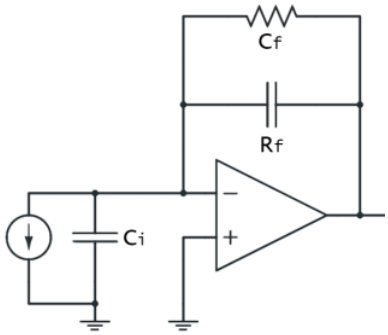

Figure 4.3: Photodiode model and transimpedance amplifier. Here Ci = 80pF.

The feedback resistor Rf is set to 820kΩ. This is the biggest value that does not result in saturation with daylight. The following equations help to design a maximally flat response with good phase margin.

$$C_f = \sqrt{\frac{C_i}{\pi R_f GBW}} \qquad f_{3db} = \sqrt{\frac{GBW}{2\pi R_f (C_i + C_f)}}$$

With $GBW = 24Mhz$, $R_f = 820k\Omega$, $C_i = 80pF$, the shunt capacitance value is $C_f = 1pF$ and the cutoff frequency is $f_{3db} = 240kHz$. The cutoff frequency is higher than what is required, but stray capacitance will probably lower that value in the real circuit.

After the first stage, the signal needs to be filtered. A high pass filter will remove the DC component and a low pass filter will help filter some noise. The same low pass filter is added after the second amplifier stage.

High pass filter	
R	3300Ω
C	12nF
f3db	4.0 kHz

1st low pass filter	
R	5600Ω
C	68pF
f3db	417.9 kHz

2nd low pass filter	
R	5600Ω
C	68pf
f3db	417.9 kHz

Table 4.2: R and C values for the different filters

As can be seen in table 4.2, the cutoff frequency of the low pass filters is higher than the maximal frequency shown in table 4.1, however by cascading the two filters and accounting for the rolloff of the first and second stage amplifier, the cutoff frequency will be lower. The theoretical frequency response will be compared with the real one in 4.1.4.

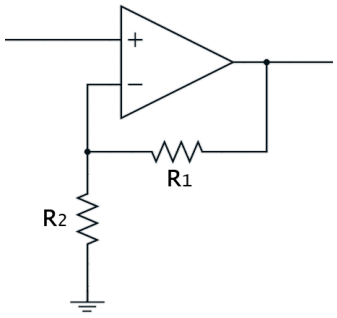

Figure 4.4: Non-inverting operation amplifier. The gain is $1 + R_1/R_2$.

The second stage gain is set to 48 by choosing $R_1 = 47k\Omega$ and $R_2 = 1k\Omega$. With this gain, the cutoff frequency of the amplifier is 24MHz/48 = 500kHz, which is sufficient.

To create an adjustable voltage reference for the comparator, a 20kΩ trimmer is added. Finally, all active components are bypassed with 100nF capacitors and a single 10μF capacitor is added on each board for avoiding larger voltage drops. The complete schematics are available in the annexes.

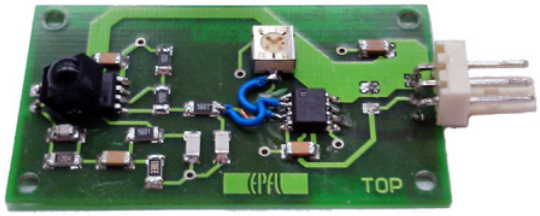

Figure 4.5: Detector circuit

4.1.4 Frequency response evaluation

A model of the circuit was established in MATLAB and compared to experimental values. Figure 4.6 shows that there is some difference. Especially critical is the difference at higher frequencies. The modeled cutoff frequency is 160kHz and the measured one is around 100kHz, significantly lower. Additional stray capacitance in the feedback network of the transimpedance amplifier (first stage) could explain the lower cutoff frequency. Typical stray capacitance for SMD components is 0.3pF, thus the shunt capacity would be 1.6pF (resistor + capacitor) and not 1pF as planned. To confirm this, the feedback capacitance should be removed or replaced with a lower value and the frequency response test should be repeated. The rest of the work was done with the circuit as designed, with the limited bandwidth (100kHz cutoff).

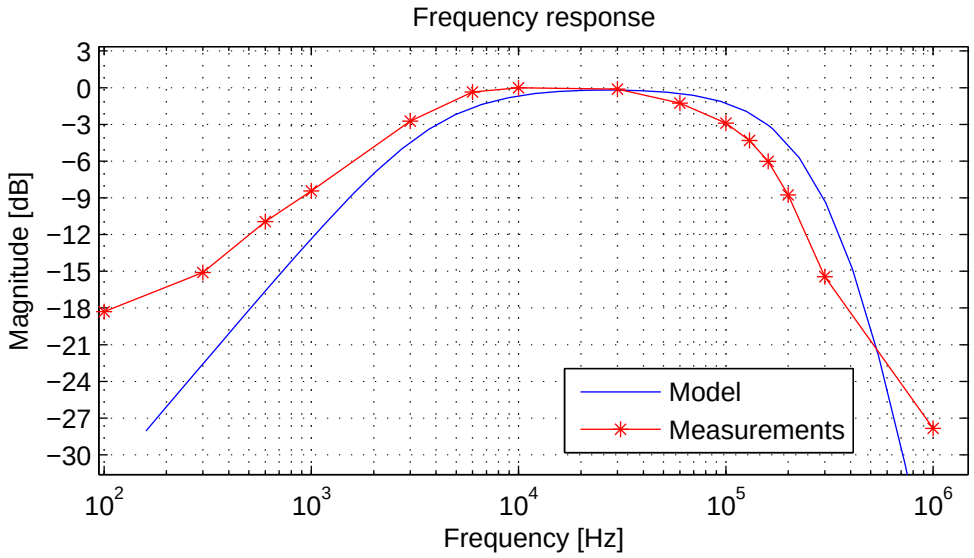

Figure 4.6: Comparison between the modeled frequency response and the measured frequency response.

4.1.5 Detection range evaluation

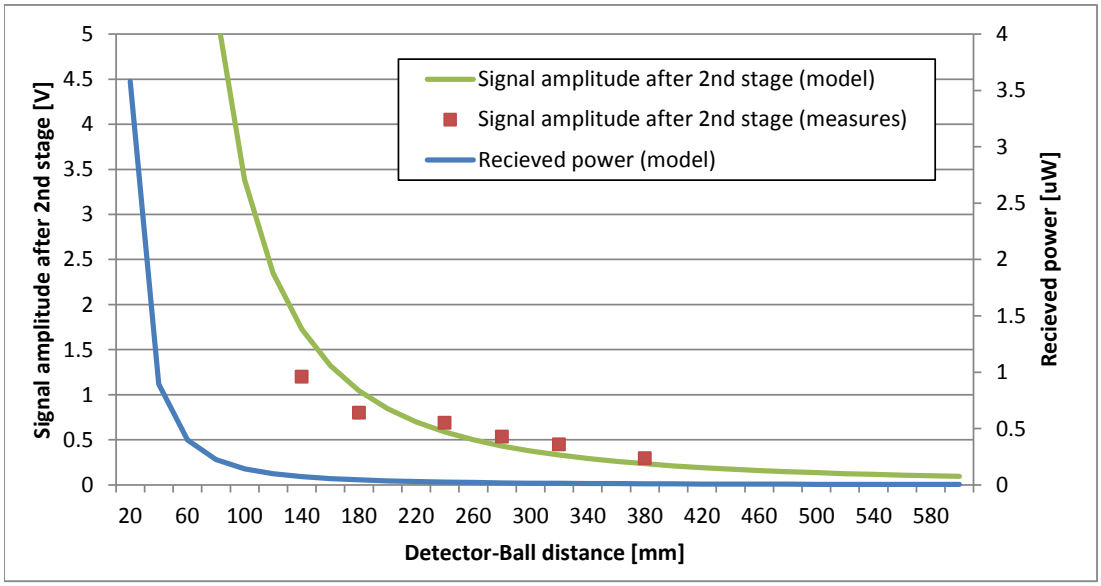

Figure 4.7: Models of the recieved power and signal amplitude and experimental values.

The optical power recieved on the photodiode and corresponding signal amplitude is modeled as a function of distance to the ball. For distances inferior to 80mm the second stage amplifier could saturate (over 5V) but this problem can be avoided if the detector circuit is placed under the table as shown in figure 4.2. Saturation can lead to wrong measurements as the amplifier needs a certain time (recovery time) to work properly again.

In the test setup, the circuit was able to detect the ball for distances up to approx. 350mm. For higher distances the signal is too faint and covered in the ambient noise (fluorescent lighting, parasite reflections, electronic noise...). To improve the detection range a retro-reflective paint was applied on a ball but it did not help.

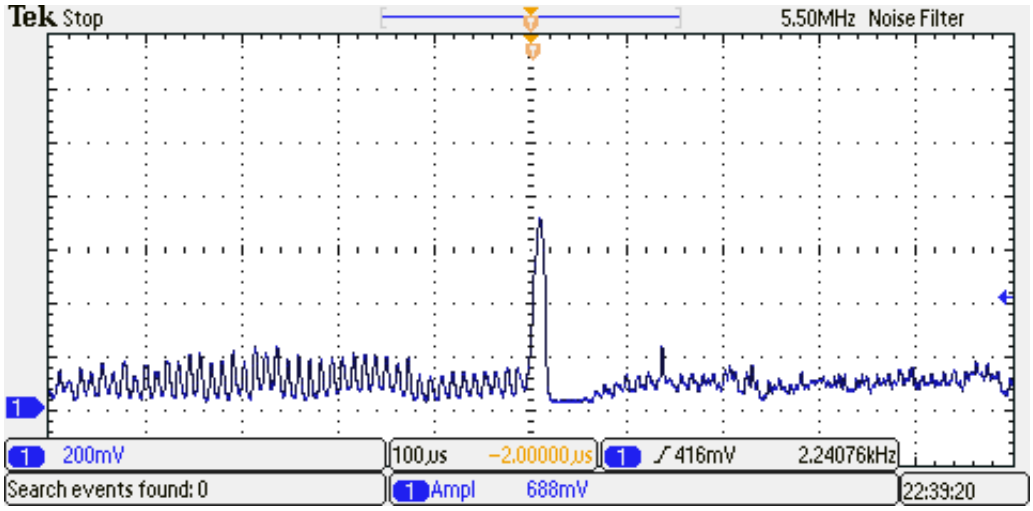

Figure 4.8: Signal after the second amplifier. The distance is 250 mm.

4.2 Start and stop of measurement triggers circuit

The start and stop triggers circuit converts the current produced by the trigger photodiodes into a signal readable by the controller. This circuit has less constraints than the detector circuit because the trigger photodiodes are directly hit by the laser beam. It consists of two detector circuits on the same board, with components dimensioned accordingly. Overall, because the recieved power is much higher, the gain is lower, the bandwidth higher and less problems were encountered. No complete study of the performance of this circuit has been done. The complete schematics with the values chosen for all the components are available in the annexes.

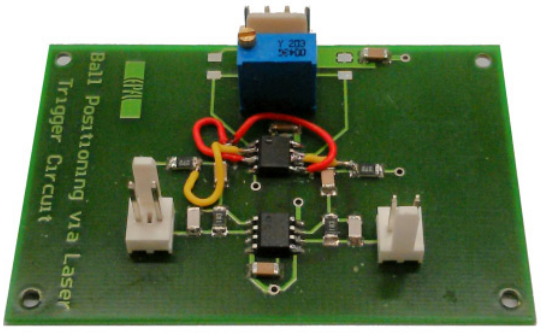

Figure 4.9: Trigger circuit

5 Controller

5.1 Tasks

The purpose of the controller is to command both laser scanners (switch between the two to avoid interferences), do the timing between all the measured light pulses, compute the angles and send them to the computer as a voltage using the integrated digital-to-analog converter (DAC).

5.2 Choice of microcontroller

For simplicity a complete board is chosen. The microcontroller needs to be sufficiently fast to do all the tasks within one scan sequence, approximately 1 milisecond. A suitable choice is the STM32VL discovery board by STMicroelectronics. It has an ARM Cortex-M3 processor clocked at 24 MHz that provides enough computational power and has an integrated DAC. The board also provides a USB link to program and debug the microcontroller. While almost all I/O pins are 5V tolerant, this microcontroller works with 3.3V. This means a converter is needed to command the laser scanners, which work with 5V. A UDN2983 chip is used for this. A board interfacing the microcontroller board with the different laser scanners, detector and trigger circuits, computer and power supply is made, a schematic is available in the annexes.

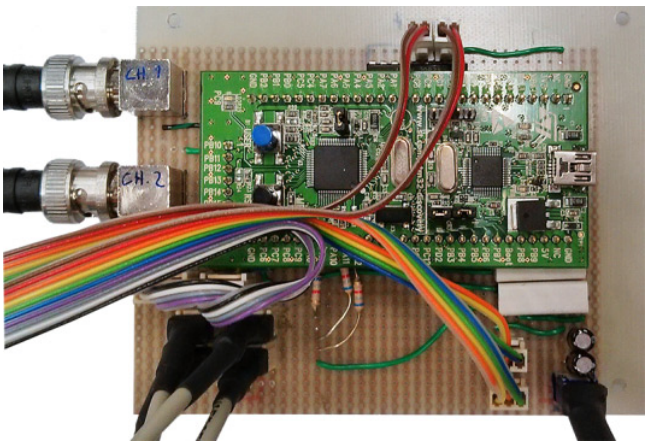

Figure 5.1: Microcontroller interfaced with the other components.

5.3 Implementation

The code running on the microcontroller can be decomposed in the following flowchart :

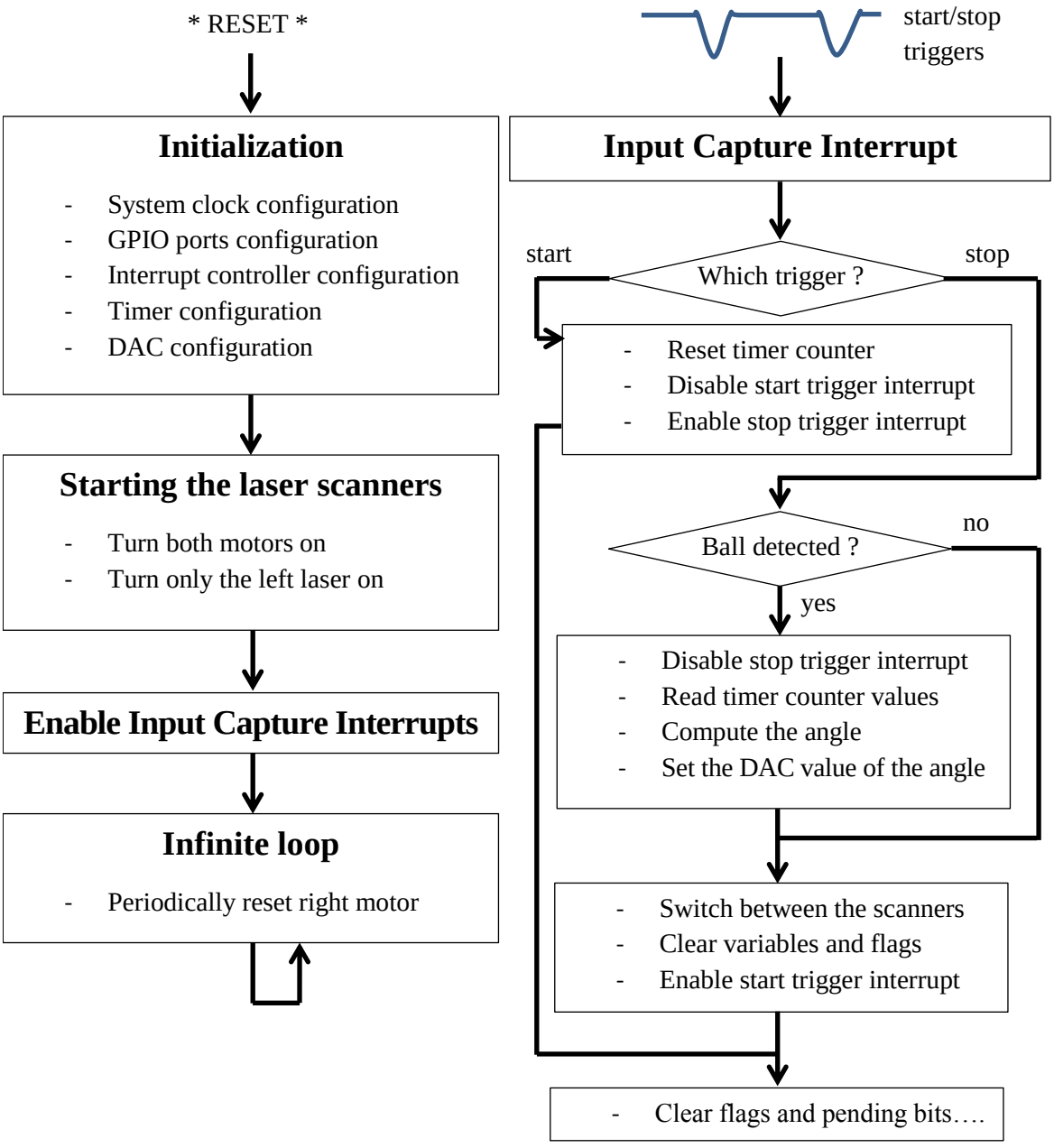

Figure 5.2: Structure of the code

The input capture feature is used to get precise time measurements of the different pulses. This system is independent of the code running on the microcontroller and the timings can be accessed later in time when necessary.

5.4 Angle calculations

The following formula is used to calculate the angle :

$$int \quad ratio = \frac{10000 \cdot (ball\_start + ball\_stop)}{2 \cdot stop\_trig}$$

The average between the falling and rising edge of the ball pulse is divided by the total scan time (from the start trigger to the stop trigger). To keep the computational time low, the calculations are done using fixed point instead of floating point numbers. This value, called *ratio* in the code, is between 0 and 10000. From this *ratio* is done the calibration of the system, which consists in finding how many units of *ratio* corresponds to one degree and then only keeping values between -10° and 90° for *alpha* and *beta*, the angles. The variables *alpha* and *beta* are then multiplied by a coefficient to get values between 0 and 4095 that can be used with the 12 bits DAC.

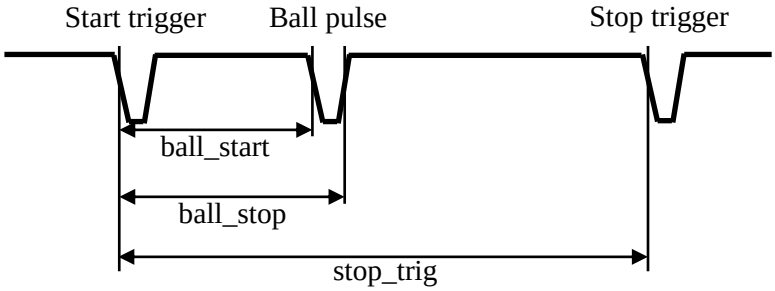

Figure 5.3: Timings between different pulses

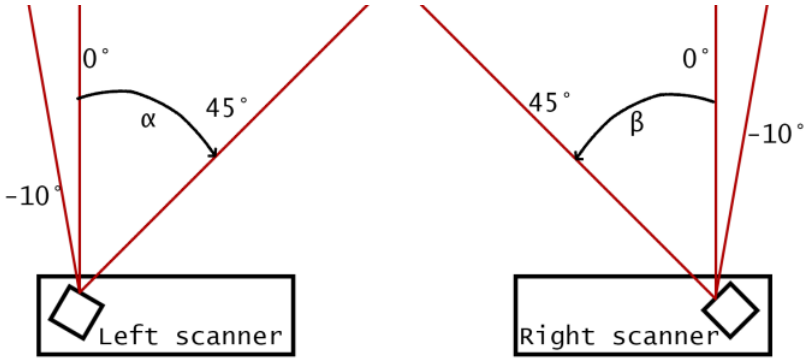

Figure 5.4: Convention used for the angles

In order to cover (almost) all the babyfoot table, the angles α and β are going from -10° to 90°. -10° is chosen because the scanners cannot be mounted exactly in the corner of the table. The ball is placed at different known angles and the system is calibrated using the different *ratio* values obtained. The exact calculations are visible in the code and in the calibration document (annexes).

5.5 Position triangulation

To get the x,y coordinates of the ball the following formulas are used :

$$b_y = \frac{\Delta x}{tan(\alpha) + tan(\beta)} \qquad b_x = b_y \cdot tan(\alpha)$$

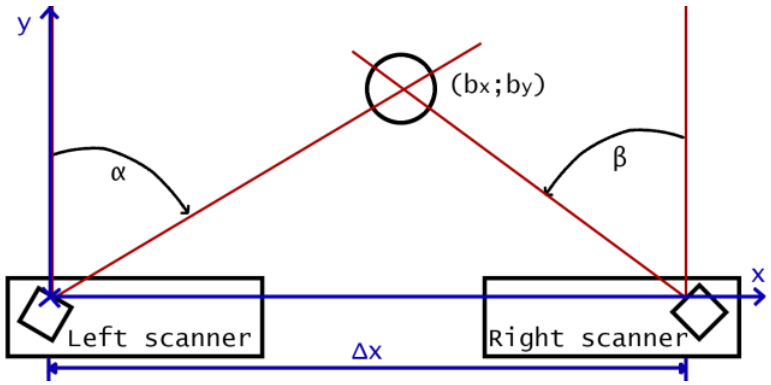

Figure 5.5: Convention used for the x,y coordinates

The triangulation is done on the computer using LabVIEW.

6 System performance evaluation

6.1 Test setup

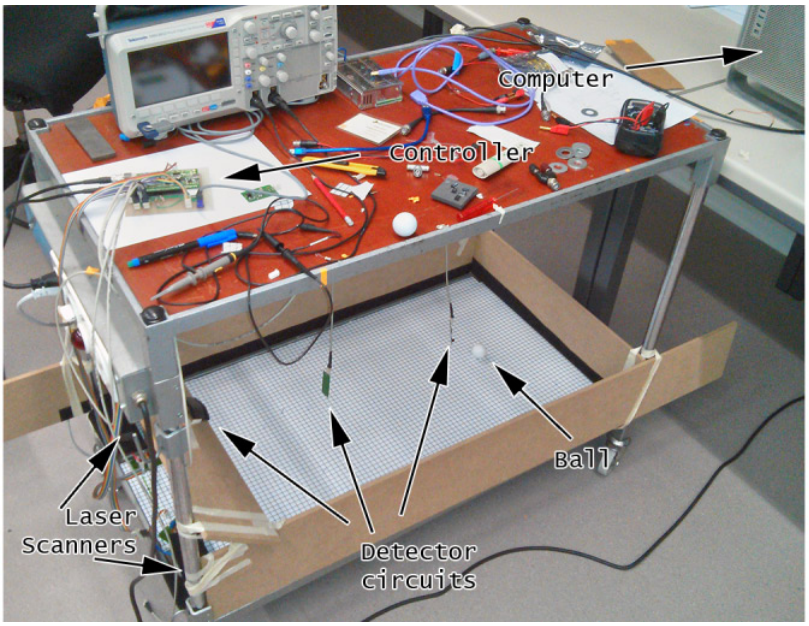

Figure 6.1: Test setup.

The test setup is a slightly smaller version of a babyfoot table. The sides are made of wood planks and some light absorbing black felt is put around the table to absorb the laser beam. The laser scanners are placed in the corners on one side of the table and mutliple detectors are placed over the table to cover the biggest area possible. The dimensions of the table are 520mm x 920mm. A centimeter squared paper is put on the surface to help calibrate and evaluate the accuracy of the system. The DAC outputs of the controller are read using a National Instruments DAQ card and LabVIEW. All the measurements shown in this chapter are done with all the fluorescent lights off, only with natural daylight.

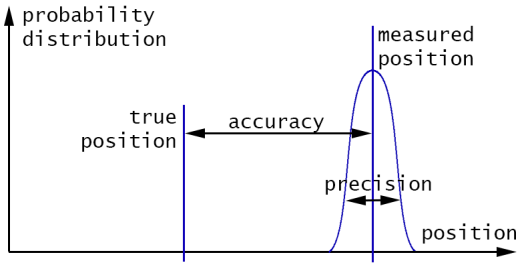

Figure 6.2: Definition of accuracy and precision

6.2 Precision

The precision of the system is estimated by doing multiple measures of the same position. Figure 6.3 shows the measuremens distribution for detector-ball distances of 100mm and 150mm. The precision is better along the x axis, but this is expected, as it covers a smaller range than the y axis (x axis : 520mm; y axis : 920mm).

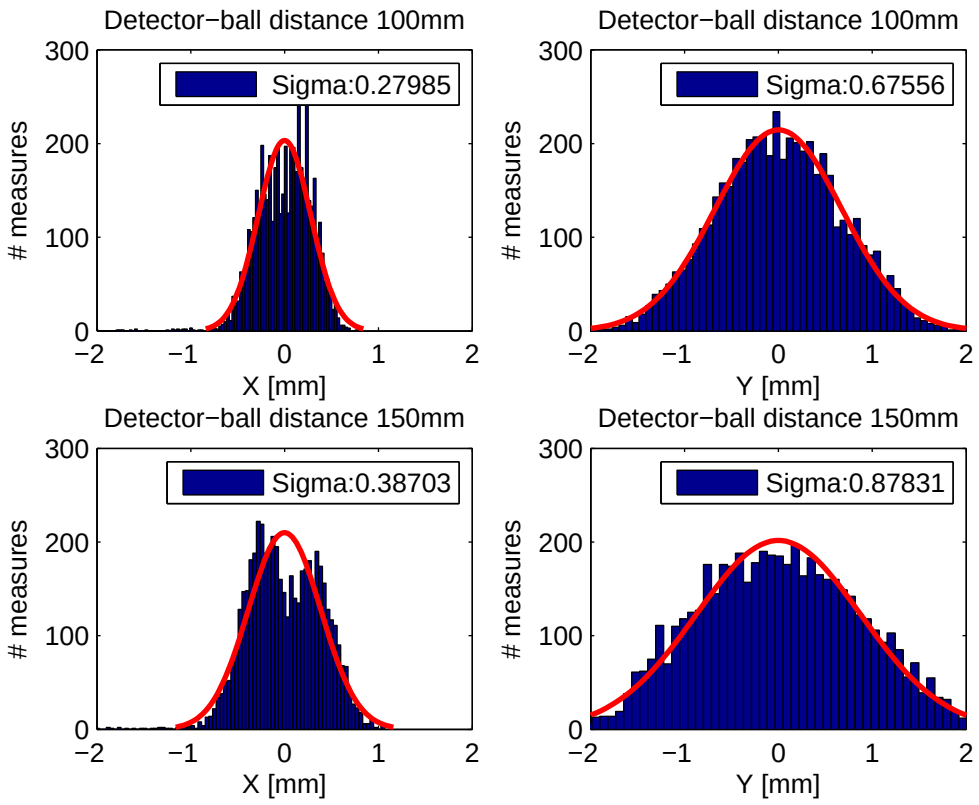

Figure 6.3: Histograms of x and y positions for detector-ball distances of 100mm and 150mm. 5000 position measurements (10 seconds @ 500Hz). Normal curves are fitted and the standard deviation is shown. The ball was placed at X=200mm, Y=400mm, here the mean is centered on 0 for ease of viewing.

When the detector is further away from the ball, more false measurements happen,

see figure 6.4. For a distance 250mm there's still a big majority of good measurements, but for 350mm and 400mm the distribution shows two peaks. One peak is made of good measurements while the other is the result of wrong measures (no ball detected). Adding a Kalman filter could probably improve the results.

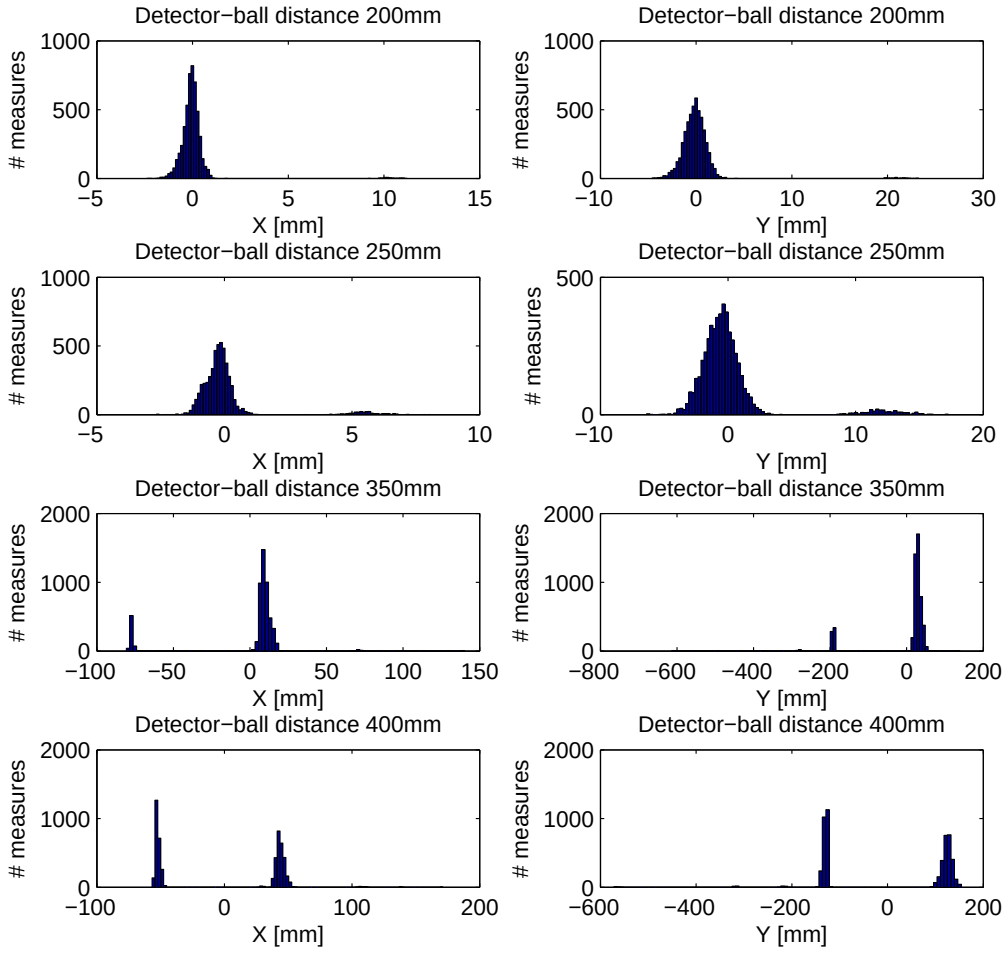

Figure 6.4: Histograms of x and y positions for detector-ball distances of 200mm and 250mm, 350mm and 400mm. 5000 position measurements (10 seconds @ 500Hz). The ball was placed at X=200mm, Y=400mm, here the mean is centered on 0 for ease of viewing.

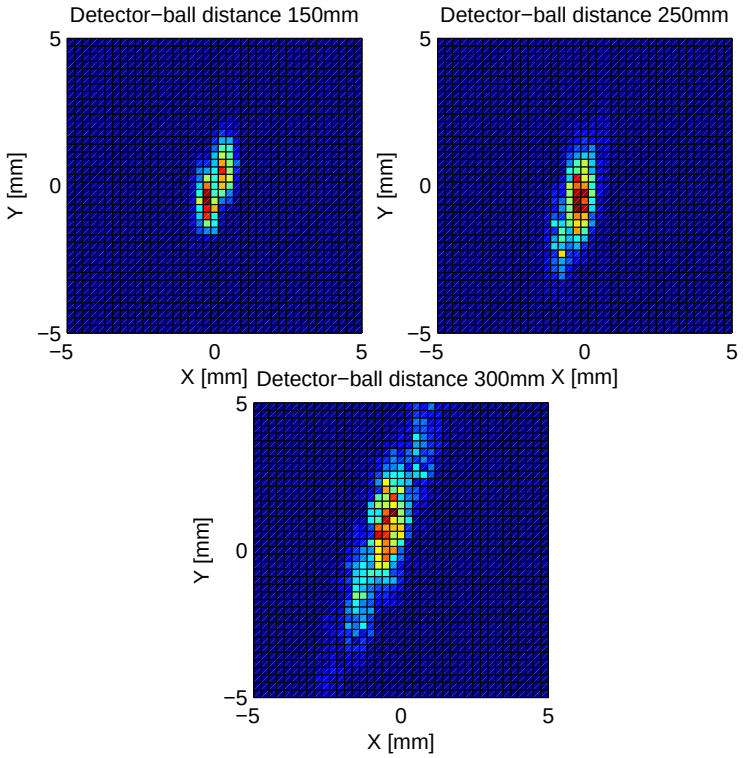

Figure 6.5: 2D Histrograms of the measurements distribution for different detector distances. 5000 position measurements (10 seconds @ 500Hz). The ball was placed at X=200mm, Y=400mm, here the mean is centered on 0 for ease of viewing.

6.3 Accuracy

Table 6.1 shows the accuracy for different positions. The accuracy of the system is not good but this is probably due to bad calibration. A careful calibration with a better method should hopefully improve this.

True X	True Y	Measured X*	Measured Y*	Accuracy X	Accuracy Y
200	200	202.7	213.1	2.7	13.1
300	600	323.4	675.1	23.4	75.1
400	700	440.1	803.9	40.1	103.9

Table 6.1: True and measured position, and corresponding accuracy, all values in milimeters. 5000 measurements @500Hz per position. [*] mean value.

6.4 Robustness

A seen in 6.2, the precision can be very good if the distance between the detector and the ball is short. For higher distances the measurements get worse quickly. A big source of problems is noise in the infrared band the system is working with. Fluorescent lights in the room generate enough noise to make any measurement impossible. Computer (and oscilloscope) screens using a fluorescent backlight are also a source of problems.

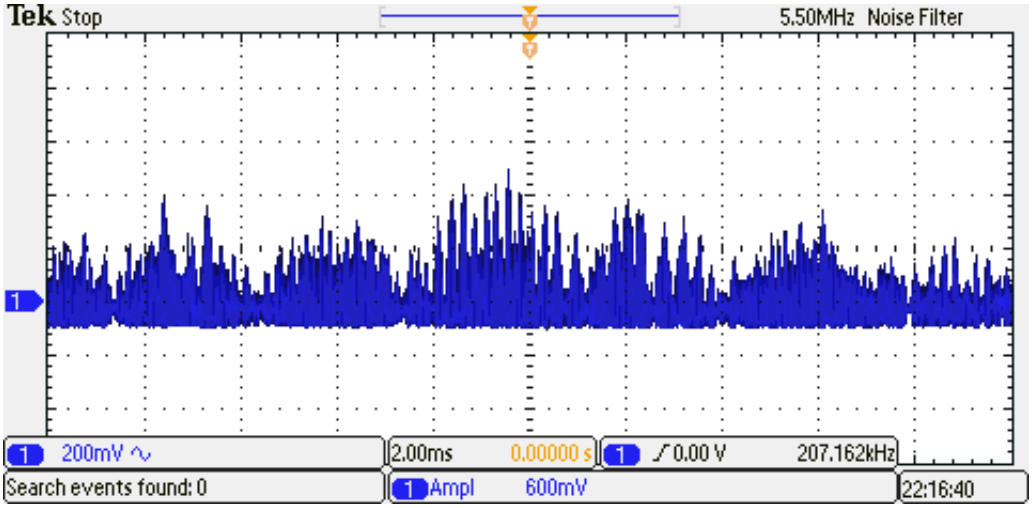

Figure 6.6: Typical noise when the fluorescent lights are on. Compare this with figure 4.8 , when all artificial lights are off.

Another source of problems is parasite reflections, as already said in 4.1.5. The black felt placed around the table to block the laser beam does not absorb 100% of the IR light. Even though it looks completely black to the human eye, it does not absorb everything in the near-IR spectrum. In ideal conditions (no fluorescent lights) the detection range of the detector circuits is limited by that parasite reflection. A parasite reflection near the detector has more intensity on the photodiode than the reflection of the ball far away, even tough the reflectivity of the ball is much higher.

Figure 6.7 shows what can be obtained in good conditions. Towards the right of the trajectory some bad measurements can be seen, due to the limited detection range of the detector circuits.

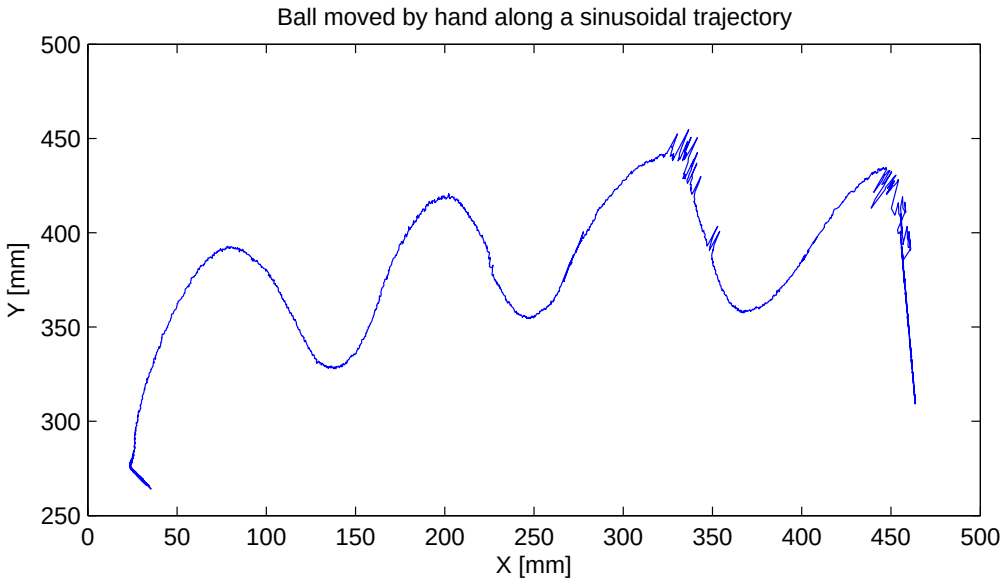

Figure 6.7: Example of a measured ball movement, all artificial lights off. (Measurement speed : 500Hz)

7 Further work

The biggest challenge in the current system is to obtain a reliable detection of the reflection of the laser beam on the ball. Using a laser with higher power is not an option, only the detection can be improved. A photodiode with a narrower band-pass filter might filter out some noise. The Vishay BPV22F photodiode might be a good choice, but requires a change of laser wavelength. Also possible is the use of seperate band-pass filters, but the incidence angle might be a limitation. Using a phototransistor instead of a photodiode is also an option. In general, the detector circuit should be revised and improved.

On the software side, calibration needs to be improved. To do this, instead of using triangulation, a possibility would be to use a look-up table directly linking *ratio* values with positions. The feasibility of this has not been studied in depth. Also, adding a Kalman filter should improve the results.

A more complete laser safety evaluation should also be done if the system is to be integrated someday in the babyfoot.

8 Conclusion

The goal was to explore the possibiliy of using laser scanners to build a high-speed ball-tracking system. This project is a proof-of-concept, showing that it is possible, but not without some difficulties. The hardware of the system and a test setup is designed and built, and the performance of the system is evaluated. The results show that the system can give very precise measurements if the ball is within a certain distance from the detector circuits.

Even tough the realization of the whole system took a lot of time, it was very interesting and nice to carry out the whole process and obtain a working tracking system.

Acknowledgments

I would like to thank Christophe Salzmann for his help with LabVIEW, Francis Tschantz for his availability and assistance with the electronics and Tomasz Gorecki and Milan Korda for their precious input.

Bibliography and links

- K. Kundert, "Power Supply Noise Reduction", The Designer's Guide Community, `http://www.designers-guide.org/Design/bypassing.pdf`
- Transimpedance amplifiers, `http://jensign.com/transimpedance/index.html`
- "Use of class 3B and 4 lasers (Internal directive LA-1-2008)", EPFL, `http://sb-sst.epfl.ch/page-22924-en.html`
- G. Brown, "Discovering the STM32 Microcontroller", `http://www.cs.indiana.edu/~geobrown/book.pdf`
- Coocox, free IDE for ARM Cortex microcontrollers, `http://www.coocox.org/`

Annexes

- Documents :
  - Complete system dimensioning (spreadsheet)
  - Calibration
- Electronics :
  - Schematics
  - PCB files
  - Datasheets
  - Source code
- Mechanics :
  - CAD Files
  - Drawings